Computers in Biology and Medicine 121 (2020) 103807

Contents lists available at ScienceDirect

Computers in Biology and Medicine

journal homepage: http://www.elsevier.com/locate/compbiomed

# Electro-thermal therapy: Microsecond duration pulsed electric field tissue ablation with dynamic temperature control algorithms

Michael B. Sano [a,*], Ross A. Petrella [a], Jacob D. Kaufman [a], Christopher C. Fesmire [a], Lei Xing [b], David Gerber [c], Callie A. Fogle [d]

[a] UNC/ NCSU Joint Department of Biomedical Engineering, Raleigh, NC, USA
[b] Stanford University School of Medicine, Division of Radiation Physics, Stanford, CA, USA
[c] Division of Abdominal Transplantation, Department of Surgery, University of North Carolina School of Medicine, Chapel Hill, NC, USA
[d] Department of Clinical Sciences and Population Health & Pathobiology, North Carolina State University College of Veterinary Medicine, USA

ARTICLE INFO

*Keywords:*
Cancer therapy
Irreversible electroporation
Thermal ablation
H-FIRE
NK-IRE

ABSTRACT

Electro-thermal therapy (ETT) is a new cancer treatment modality which combines the use of high voltage pulsed electric fields, dynamic energy delivery rates, and closed loop thermal control algorithms to rapidly and reproducibly create focal ablations. This study examines the ablative potential and profile of pulsed electric field treatments delivered in conjunction with precise temperature control algorithms. An *ex vivo* perfused liver model was utilized to demonstrate the capability of 5000 V 2 μs duration bipolar electrical pulses and dynamic temperature control algorithms to produce ablations. Using a three applicator array, 4 cm ablation zones were created in under 27 min. In this configuration, the algorithms were able to rapidly achieve and maintain temperatures of 80 °C at the tissue-electrode interface. A simplified single applicator and grounding pad approach was used to correlate the measured ablation zones to electric field isocontours in order to determine lethal electric field thresholds of 708 V/cm and 867 V/cm for 45 °C and 60 °C treatments, respectively. These results establish ETT as a viable method for hepatic tumor treatment with ablation profiles equivalent to other energy based techniques. The single applicator and multi-applicator approaches demonstrated may enable the treatment of complex tumor geometries. The flexibility of ETT temperature control yields a malleable intervention which gives clinicians robust control over the ablation modality, treatment time, and safety profile.

## 1. Introduction

The lack of viable, transplantable livers as well as a poor response to chemotherapy and radiation has resulted in a growing interest in the development of techniques for the in situ tissue destruction (ablation) of hepatic tumors. The devices currently being investigated for hepatic tumor ablation have been categorized as being either thermal or non-thermal based on their biophysical method of killing cells [1]. The thermal techniques are most notably radio frequency ablation (RFA) and microwave ablation (MWA) which use periodic electric currents and electromagnetic fields, respectively, to induce a durable thermal injury zone. Due to the temperature dependent method of tumor destruction, both RFA and MWA have been contraindicated for tumors near the gastrointestinal tract, biliary system, and heart as well those that occur within 1 cm proximity to major blood vessels (e.g. the hepatic portal tract) [2] unless additional techniques (hydrodissection [3], thermoprotective agents [4], or physical tissue separation) are implemented. To enable the treatment of tumors which involve the hepatic veins, inferior vena cava, and biliary tract, a new therapy known as irreversible electroporation (IRE) which causes the permanent rupturing of the cell membrane by exposure to high intensity pulsed electric fields, has been developed [5]. Irreversible electroporation is currently FDA approved for soft tissue ablation via the NanoKnife ablation system (NK-IRE).

NK-IRE has been designated as being non-thermal in its method for killing tumor cells [6–11]. However, in practice there is a tradeoff between treatment time and deleterious tissue heating. There can be either long treatments with relatively little change in tissue temperature or short treatments with a rapid increase in tissue temperature [12]. The demands of a human clinical environment typically limit the use of NK-IRE to smaller tumors (<3 cm) for which energy delivery can be completed within 35 min [13]. NK-IRE pulses must be delivered with

* Corresponding author.
*E-mail address:* mikesano@med.unc.edu (M.B. Sano).

https://doi.org/10.1016/j.compbiomed.2020.103807
Received 19 August 2019; Received in revised form 27 April 2020; Accepted 2 May 2020
Available online 11 May 2020

cardiac synchronization [14,15] due to the induction of severe muscle contractions [16] and therefore protocols tend to favor the use of longer duration electrical pulses (50–100 μs) to maximize the energy delivery rate and reduce the overall treatment time. However, NK-IRE parameter selection including the pulse width, voltage-to-distance ratio, and total number of pulses delivered can have a dramatic effect on the extent of thermal injury produced by the induced Joule heating of the tissue [17]. In perhaps an attempt to limit these unwanted thermal effects, the clinical tool limits maximal pulse amplitudes to 3000 V and currents to 50 A [13] which combined with treatment time constraints limits the overall size of tumors which can be effectively ablated.

The use of shorter (0.25–5.0 μs) alternating polarity electrical pulses known as high frequency irreversible electroporation (H-FIRE) have been proposed as a potential solution to the challenges associate with NK-IRE [18–20]. However, in order to have equivalent ablation diameters the voltage applied will likely need to exceed 3000 V [12,21,22] due to the necessity of higher electric fields to induce equivalent ablation zones and Joule heating still persists with these waveforms [12].

While adverse outcomes due to thermal injury are rare with NK-IRE, the use of higher voltages in pursuit of larger and more rapid ablations may increase their occurrence. Fortunately, unwanted thermal injury is potentially avoidable altogether with proper engineering controls designed to manage the intra-tumor environment during the pulsed electric field treatment. Within a control systems perspective, NK-IRE and H-FIRE therapies are both open loop being devoid of any feedback mechanism based on a process variable. They do not consider any in situ environmental conditions. Therefore, temperature is allowed to increase unrestricted throughout the treatment time period.

Electro-thermal therapy (ETT) is a potential solution as the first controlled method for automated adjustments of pulse delivery rate for temperature regulation of an ablation region [23]. Traditional H-FIRE treatments use 100–200 μs bursts of pulses delivered at a specified frequency [20,24]. In contrast, ETT employs a continuous pulse delivery scheme that adjusts the delay between sequential waveforms based on real time temperature measurements. This enables ETT to be both truly non-thermal and controllably thermal. For non-thermal treatments, ETT allows for the shortest treatment times while mitigating thermal damage to the patient. In a controllably thermal configuration, ETT could allow for clinicians to determine the extent of thermal damage that a tumor receives. Alternatively, a temperature control point can be placed near to tissue that ought to be preserved after treatment. This allows for safer operation near critical structures with potential for reduced side effects.

In this study we demonstrate ETT as a control schema to maximize pulse delivery rates, minimize treatment times, and provide a mechanism for clinicians to control thermally and electrically induced ablative outcomes. An *ex vivo* perfused liver model was used to demonstrate the use of dynamic temperature control algorithms to produce 4 cm ablation zones in under 27 min with a three applicator array. In separate experiments, these algorithms were able to rapidly achieve and maintain temperatures of 45, 60, or 80 °C at the tissue-electrode interface. A single applicator approach was used to correlate the measured ablation zones to electric field isocontours in order to determine a lethal electric field thresholds for ETT treatments of 708 V/cm and 867 V/cm for 45 °C and 60 °C ETT treatments, respectively. These results establish ETT as a viable method for hepatic tumor treatment with ablation profiles equivalent to other energy based ablation techniques.

## 2. Methods and procedures

### 2.1. Tissue preparation and processing

All experiments were conducted on *ex vivo* porcine livers following a previously established technique for organ preservation [25] and which enables ablation assessment at time points between 2 [25,26] and 24 h [27,28] post treatment. Livers obtained from a local slaughter house within 30 min of euthanasia were flushed with 200 mL of 1x Phosphate Buffered Saline (PBS) (IS25049, Aldon Corp. Avon NY) to remove large blood clots then transported on ice to the laboratory. A peristaltic pump (EW-77921-65, Cole-Palmer, Vernon Hills, IL) was attached to the liver hepatofugally via the vena cava and perfusion with PBS was initiated using a flow rate between 18 and 25 mL/h. To simulate venous pressure and increase the volume of fluid within the organ the flow of perfusate exiting the portal vein was restricted via a plastic luer lock (4551100, Cole-Palmer, Vernon Hills, IL) coupled to 1 mm inner diameter tubing. To facilitate the removal of any potential blood clots the liver was gently massaged and continuously perfused until tissue blanching occurred indicating that the organ had been flushed and all lobes were receiving PBS. Finally, the existing perfusate was discarded and replaced with fresh PBS which was occasionally refreshed during the experiments.

Post-treatment the organs were moved to a standard laboratory refrigerator at 4 °C and perfused overnight (10–15 h). This duration was chosen to allow for delayed cell death processes associated with the treatment to occur while remaining within the 2 [25] – 24 [27] hour window for which this technique has been previously validated. For the three applicator array (3AA) protocol, treatment sites were identified and sectioned by hand perpendicular to applicator insertion in 0.5–1.0 cm thick slices. This yielded between six and ten measurable ablation zones per treatment site. For the single applicator and grounding pad (A + GP) protocols, a single section was made parallel to and along the applicator insertion path yielding two measurable tissue sections and four measurements (2x height and 2x width) per treatment site. To enhance contrast between live and dead tissue for publication, the tissue sections were placed in a bath containing 10 g/L triphenyl tetrazolium chloride (TTC, A1087009, Alfa Aesar, Tewksbury, MA) in PBS overnight in a dark environment (Supplemental Fig. 1). TTC enzymatically reduces into red 1,3,5-triphenylformazan in living cells and excluded from dead cells. Further contrast enhancement was achieved by preserving tissue samples in Neutral Buffered Formalin (22-046-361, Thermo-Fisher Scientific, Waltham, MA), however, the results of these process were variable and required deviation from previously published methods [25] to achieve suitable results. Ablation zones, indicated by a change in tissue color and texture [25], were measured using digital calipers [29]. For the three applicator array, three measurements for each ablation zone were obtained by identifying a straight line connecting the punctures of adjacent applicator pairs then measuring the ablation margin along that line. For the single applicator and grounding pad protocol, the maximal length along the applicator insertion path and maximal width perpendicular to the applicator insertion path were recorded for each ablation zone [12,28]. The length and width values for ablations within treatment groups were averaged to determine the mean ablation size and data is presented as mean ± standard deviation.

### 2.2. Energy delivery

ETT waveforms (Fig. 1a) were delivered to the liver tissue via 1 mm diameter applicators (Monopolar Probe, AngioDynamics Inc., Latham, NY) which contain an adjustable insulator used to set the length of the exposed electrode (Fig. 1b). Ablations were created using two distinct applicator configurations (see Table 1): (1) A three applicator array (3AA, Fig. 1c) consisting of three applicators in a triangular pattern with 3 cm center-to-center spacing and 3 cm electrode exposures (N = 4 replicates). (2) An applicator and grounding pad configuration (A + GP) utilizing a single applicator with 1 cm of electrode exposure and a 4 × 5 cm aluminum grounding pad placed under the organ (N = 3 replicates). These configurations were selected to (1) demonstrate the feasibility of creating clinically relevant ablations and (2) enable the determination of lethal electric field thresholds through the use of a simplified geometry, respectively.

All experiments were conducted using a continuous pulse delivery protocol (Fig. 1a). A bipolar waveform consisting of a positive polarity 2 μs pulse, a 5 μs delay, and a 2 μs negative polarity pulse (2-5-2 waveform) was repeated to deliver a specified electrical dose with an

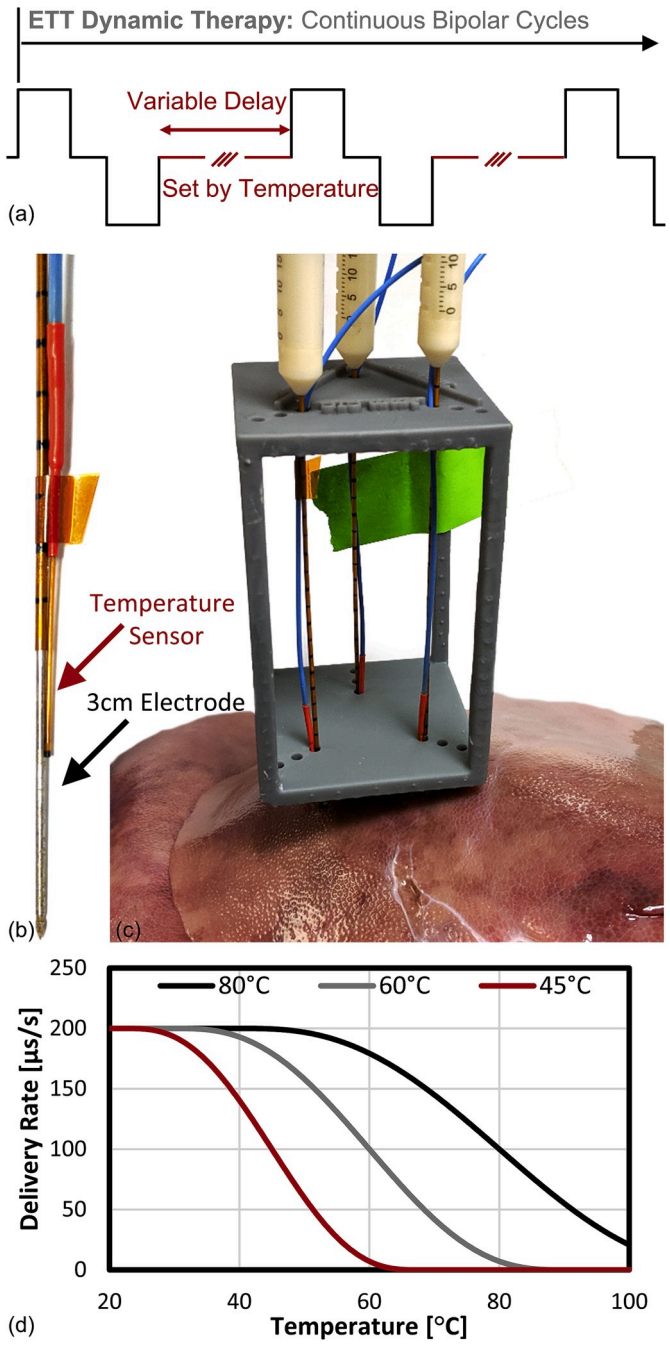


**Fig. 1.** ETT utilizes a dynamic energy delivery scheme to adjust treatment parameters in real time to respond to changing tissue conditions. (a) The delay between successive ETT waveforms is modulated based on measurements from a (b) temperature sensor attached to the electrode applicator. Treatments are through a single applicator and grounding pad or (c) through probe pairs in multi-applicator arrays. (d) The dynamic energy delivery rate is dependent on a number of factors including the maximum prescribed rate and the target temperature.

integrated energized time (IET) calculated as:

$$IET = \sum_{0}^{N} (\tau_p + \tau_n)\ [s] \tag{1}$$

where N is the total number of waveforms delivered and $\tau_p$ and $\tau_n$ are the positive and negative pulse durations (2 µs), respectively. The delay (δ) between sequential 2-5-2 waveforms was either held constant (0.024 s) or dynamically adjusted using a temperature control algorithm to achieve a specified energy delivery rate (R) calculated as:

$$R = \frac{\tau_p + \tau_n}{\delta}\ [\mu s / s] \tag{2}$$

### 2.3. Temperature control algorithm

In all experiments, a fiberoptic temperature sensor (TS5, Micronor Inc., Camarillo, CA) was affixed to each applicator (Fig. 1b–c) with the sensing region in contact with the exposed electrode approximately 1 cm distal from the insulation to enable measurements in the regions of anticipated maximal temperature change. Temperatures were acquired by a signal conditioner (Fotemp, Micronor Inc., Camarillo, CA), transmitted over a Serial connection, and recorded at 3 Hz using a custom Python application. This temperature value was used to determine the rate (R, Fig. 1d) at which energy was delivered:

$$R(T) = R_{max} \cdot \rho(T)\ [\mu s / s] \tag{3}$$

$$\rho(T) = 0.5 - 0.9375 \cdot \Gamma(T) + 0.625 \cdot \Gamma(T)^3 - 0.1875 \cdot \Gamma(T)^5 \tag{4}$$

$$\Gamma(T) = \frac{T - T_t}{\beta} \tag{5}$$

$$\beta = T_t * \omega \tag{6}$$

where $R_{max}$ is the maximum energy delivery rate [µs/s] prescribed, T is the instantaneous temperature [°C], $T_t$ is the target temperature [°C], and ω is a coefficient which broadens or narrows the slope between maximum and minimum energy delivery rates. Smaller values of ω result in sharper transitions between the maximum and minimum rates and can lead to oscillations and instability of the algorithm. Conversely, larger values of ω result in slower algorithmic response to temperature transients and a longer duration required to achieve target temperatures. As a compromise, ω was held constant at 0.5 for all experiments presented here. It should be noted that the temperature control algorithm, as implemented in this study, only utilized temperature data from a single user selected probe and the dominant probe was changed manually if an alternate probe exceeded the target temperature by more than 3 °C.

Electrical pulses were delivered using a custom pulse generator based on an H-Bridge topology which included a 100 MSPS data acquisition system to record voltage and current waveforms in real time. For safety, the system was designed to automatically abort treatments if the software measured average currents above 75A, the hardware detected instantaneous currents above 90A, or the average power reached 100 Watts. These events were rare and only two software mediated over current (75A) events occurred for the experiments presented here.

For each applicator configuration a single ramp-up experiment was conducted in which the voltage was sequentially increased from 250 V to 5000 V to ensure proper behavior of the pulse generator. For each additional applicator placement, the applied voltage was immediately set to 5000 V.

### 2.4. Three applicator array (3AA) treatments

Each applicator in the 3AA was manually placed in the tissue through a custom electrode holder (Fig. 1c) such that the entire 3 cm exposed electrode and 0.5 cm of insulation were below the surface of the tissue. To facilitate sectioning, the applicators were placed perpendicular to the tissue surface. To accommodate the two outputs on the pulse generator, energy was sequentially delivered between adjacent probe pairs (1–2, 2–3, 3–1). A dose of 0.02s IET (5000x waveforms, 10,000x pulses) was delivered between each pair resulting in a total dose of 0.06s IET per ablation. The system was briefly disabled between probe pairs to accommodate manual switching of the leads and treatments were

**Table 1**
Summary of experiments.

| Probe Configuration | Temperature Set Point [°C] | Probe Spacing [cm] | Probe Exposure [cm] | Electrical Dose (IET) [s] |
|---|---|---|---|---|
| 3 Applicator Array (3AA) Fig. 3 | None | 3 | 3 | 0.06 (0.02 per probe pair) |
| 3 Applicator Array (3AA) Fig. 4 | 80 | 3 | 3 | 0.06 (0.02 per probe pair) |
| Applicator + Grounding Pad (A + GP) Supplemental Fig. 4 | 45 | – | 1 | 0.02 |
| Applicator + Grounding Pad (A + GP) Supplemental Fig. 4 | 60 | – | 1 | 0.02 |

resumed as soon as safely possible.

To match the total treatment time of similar 3 applicator MWA protocols (6 min), non-temperature controlled experiments were conducted with an energy delivery rate of 166.7 μs/s. These treatments had a fixed a repetition delay of 0.024s between waveforms (0.024s · 5000x waveforms · 3 applicator pairs = 360s). Temperature controlled experiments were conducted with a target temperature of 80 °C and a maximum energy delivery rate of 166.7 μs/s. These parameters were selected to minimize treatment time and investigate the effects of energy delivery well beyond the threshold for instantaneous thermal damage.

### 2.5. Single applicator and grounding pad (A + GP) treatments

A single applicator with a 1 cm electrode exposure was inserted into the tissue such that the electrode and 0.5 cm of insulation were below the tissue surface. A 4 × 5 cm aluminum grounding pad was placed under the tissue and occasionally moved between treatments to maintain similar distances between experimental groups which aided in delivering consistent initial current amplitudes. For each applicator placement a total dose of 0.02s IET was delivered with target temperatures of either 45 °C or 60 °C. These values were chosen to investigate if temperature is a confounding factor in ablation size and lethal threshold calculations. The smaller electrode exposure utilized in this experiment resulted in less heating and a maximum energy delivery rate of 200 μs/s was utilized to improve the ability of the algorithm to achieve 60 °C temperatures.

### 2.6. Numerical prediction of lethal electric fields

COMSOL Multiphysics was used to calculate the electric field distribution within the tissue (Supplemental Fig. 2) for both experimental applicator configurations and to determine the electric field isocountours which most closely correlated with the ablation geometries. This data was then used to generate predictive models representing the anticipated treatment zones which can be expected *in vivo*. This was accomplished via routine techniques [22,30] which are described in detail in the supplemental materials. Briefly, 3D (3AA) and 2D (A + GP) Electric Currents Modules were used to calculated the steady state electric field distribution around the electrodes using a dynamic conductivity model to account for electroporative effects (details in supplemental materials). For the 3AA the electric field data along a line passing through the geometric center of two electrodes was exported to a spreadsheet. This data was then used to cross-reference the length of each ablation measurement to identify the electric field isocontour value which corresponded to the size of the ablation. For the A + GP configuration data for the electric field distributions along the lines extending parallel to and perpendicular to the center of the electrode were exported and correlated to the length and width, respectively, of the ablation zones. Lethal threshold values for each measurement within treatment groups were then averaged and data is presented as mean ± standard deviation.

For comparison, NK-IRE treatments were simulated using two and three applicator arrays with 2 cm center-to-center spacing and a 1.5 cm electrode exposure to match typical clinical practice. The lethal threshold for IRE in liver ranges from approximately 423 [27] to 637 V/cm [31] depending on the administered protocol. Electric field isocontours corresponding to 500 V/cm [10,32] were used to illustrate NK-IRE ablation zones in comparison to isocontours representing the lethal thresholds determined for ETT treatments in this study.

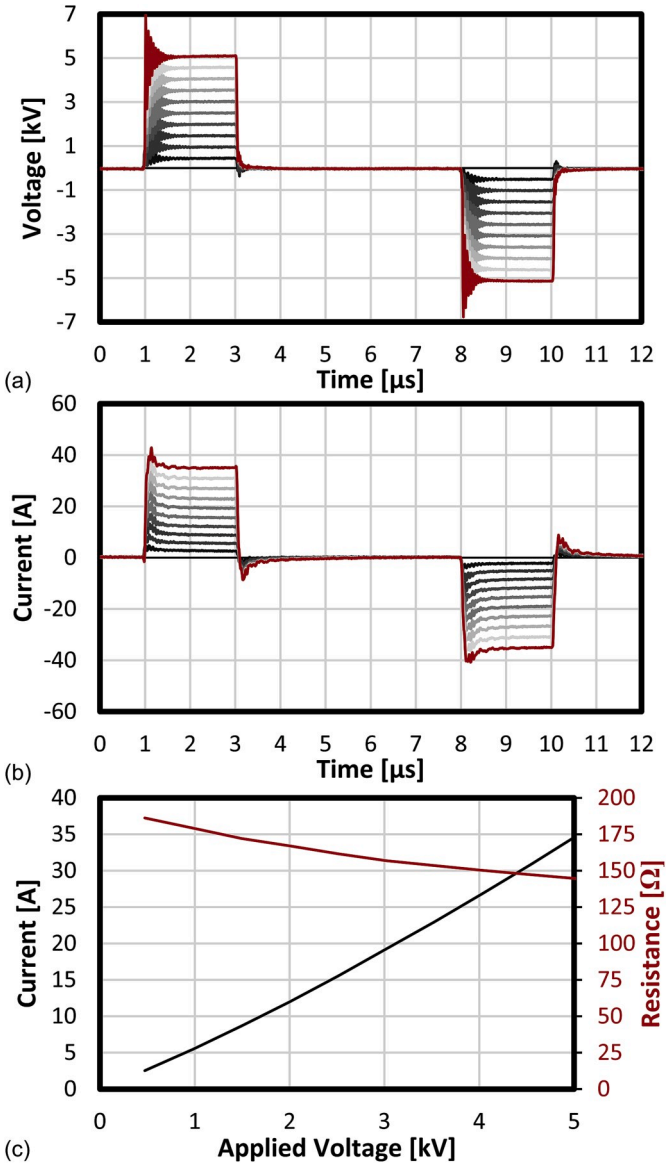


**Fig. 2.** (a) Voltage, (b) current, and (c) impedance data found during the ramp-up procedure for the 2-5-2 waveform and 3AA configuration with energy delivered between two adjacent applicators. This gradual ramp up was conducted for the first applicator placement to ensure that output currents were within the safe operating range of the pulse generator. Plot lines of the same color in (a) and (b) indicate corresponding measurements.

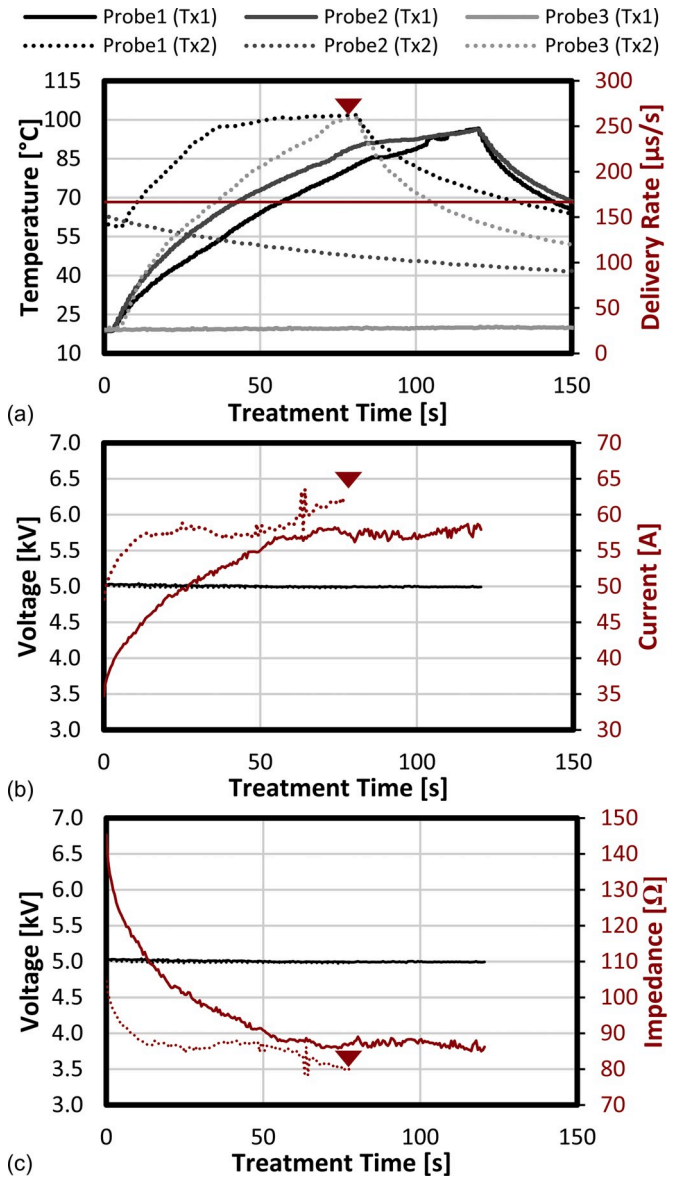


**Fig. 3.** Treatments without thermal control enabled resulted in temperatures of 100 °C. (a) Plots showing the temperature profiles when an initial 0.02s IET dose was delivered between probes 1 and 2 (solid lines) and then a second 0.02s IET dose was delivered between probes 1 and 3 (dotted lines). The initial temperature at probe 1 for the second dose was 60 °C which rapidly increased to 100 °C resulting in charring and arcing at the tissue-electrode interface at which point the treatment was aborted (red arrows). The red line in (a) indicates a constant energy delivery rate of 167 µs/s for these treatments. (b) Voltage - current and (c) voltage - impedance plots associated with the first (solid lines) and second (dashed lines) doses showing a rapid increase in current and decrease in impedance associated with energy delivery.

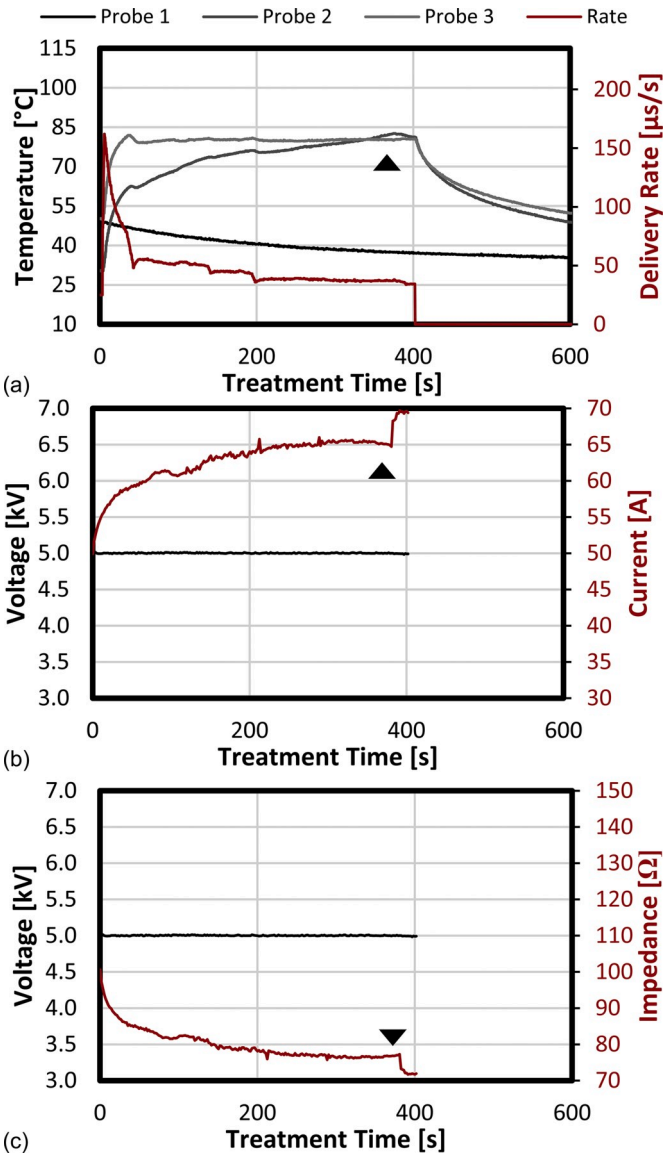


**Fig. 4.** Characteristic data from 3AA treatments with thermal control using an 80 °C temperature set point. (a) Temperature plots (greyscale lines) showing a rapid increase to the target temperature on the controlled channel (Probe 3) with minimal overshoot. The energy deliver rate (red line) decreased from a baseline of 167 µs/s to a minimum of 35 µs/s to maintain the target temperature. The temperature on an uncontrolled channel (Probe 2) briefly breached the target temperature (black arrows) resulting in a measureable change in (c) current and (d) impedance indicating a strong correlation of these parameters with tissue temperature.

## 3. Results

### 3.1. Treatment observations

Voltage (Fig. 2a) and Current (Fig. 2b) measurements taken during the ramp up protocol indicate that the impedance of untreated tissue exhibited a slight voltage dependence (Fig. 2c) which decreased from 180 to 144 Ω for pulses with amplitudes between 250 and 5000 V. Voltage and current waveforms for each pulse amplitude exhibited a moderate degree of ringing during the rising and falling edges which subsided within approximately 500 ns.

Initial treatment between the first probe pairs (probes 1 and 2) without thermal control resulted in gradual increases in temperature from baseline (20 °C, room temperature) to 96 °C (Fig. 3a solid lines) over the 0.02s IET treatment. No increase in temperature was observed for the third probe (probe 3) which was left floating. An initial current measurement of 34.7A gradually increased to 58.5 A (Fig. 3b) and impedance between the energized probe pair decreased from 145Ω to 85Ω over the course of this treatment. The measured voltage remained consistent (range: 5.05–4.98 kV) throughout.

Energy delivery between the next sequential probe pair (probes 1 and 3) resulted in a rapid increase in temperature to 100 °C (Fig. 3a dots). Soon after, visible emission of steam from the applicator insertion site was observed followed by charring and arcing at the tissue surface (results not shown) at which time the treatment was aborted (Fig. 3, arrow heads) to prevent damage to the pulse generator by stochastic

arcing and no further uncontrolled experiments were conducted. Inflection points in the current (Fig. 3b) and tissue impedance (Fig. 3c) plots approximately corresponded with timing of visual appearance of steam.

Utilization of the temperature control algorithm resulted in an increase in tissue temperatures to the target temperature with only minor overshoot before settling. Temperature profiles and energy delivery rates varied between treatments due to dynamic conditions in the perfused liver tissue and characteristic plots are shown in Fig. 4a. Treatment currents (Fig. 4b) and tissue impedance (Fig. 4c) appeared to be temperature sensitive with a dramatic change in both observed when the temperature of one probe breached the target set point (Fig. 4, black arrows). The entire temperature controlled 3AA treatments (Supplemental Fig. 1d) required 26.9 ± 8.8 min to complete compared to an estimated treatment time of 6.0 min if matched non-temperature controlled experiments were feasible.

Temperature profiles and energy delivery rates for treatments with the A + GP configuration (Supplemental Figs. 4a–b) were consistent between treatment groups. Distinct impedance changes were observed for the 45 °C and 60 °C set points (Supplemental Fig. 4c) with maximum decreases of 39.9 ± 1.6 Ω and 50.4 ± 4.7 Ω, respectively. These treatments required 5.8 ± 0.5 and 2.4 ± 0.19 min to complete.

### 3.2. Characterization of tissue ablations

Ablation zones for the 3AA (Fig. 5a) and A + GP (Fig. 5b–c) appeared lighter in color and different in texture than the surrounding unaffected tissue. An additional region of white tissue with a spongy texture indicative of thermal injury [25] was observed adjacent to the electrode in all 3AA (Supplemental Fig. 1) and 60 °C A + GP treatments (0.77 ± 0.29 cm). This was not observed in the 45 °C A + GP treatments. Ablations created with the 3AA had a distinct tri-lobe shape with indentations along the outer boundary between each applicator. The A + GP ablations were oval to circular in shape which was dependent on the sectioning location relative to the applicator insertion path. The mean ablation zones measured 3.96 ± 0.43 cm, 1.76 ± 0.021 cm, and 1.56 ± 0.34 cm for the 3AA, 45 °C A + GP, and 65 °C A + GP treatments, respectively (Fig. 5d). The mean ablation size between 45 °C and 60 °C treatments was not significantly different ($p = 0.0946$). These measurements corresponded to lethal electric field thresholds of 708 ± 108 V/cm and 867 ± 192 V/cm for the 45 °C and 65 °C A + GP treatments (Supplemental Fig. 3) which were found to be statistically significantly different ($p = 0.0242$). The 3AA treatments required the longest treatment times 26.9 ± 8.7 min due to the need to deliver energy between three different probe pairs (Fig. 5e). The A + GP treatments were completed in 5.8 ± 0.5 and 2.4 ± 0.2 min for the 45 °C and 60 °C set point treatments, respectively.

Experimentally determined ETT lethal thresholds and NK-IRE values from the literature were used to predict the ablation geometries anticipated for 2 and 3 applicator treatments (Fig. 6) when 3 kV or 5 kV treatments are administered. These simulations indicate that for a fixed voltage, ETT ablations will be smaller than those produced by NK-IRE. However, as ETT enables the use of higher treatment voltages and currents, these protocols should be capable of producing substantially larger ablations (Supplemental Fig. 5) than feasible with current clinical tools, without the need to retract or move the applicators mid-treatment.

## 4. Discussion

Temperatures in excess of 43 °C, which are capable of damaging cells and tissues [33–35], generated as a result of Joule heating could contribute to adverse side effects observed *in vivo*, earning NK-IRE a safety profile equivalent to microwave ablation, with rare examples of coagulative necrosis [17], thrombosis [36], abscesses [37], and fistulas [38] being reported in the literature. In extreme cases there is a feed-forward mechanism in which excessive temperatures desiccate the tissue, initiate charring along the electrode's insertion path, and culminates in the generation of electrical arcs [26] which can catastrophically damage and obliterate the tissue in proximity to the electrode or between a pair of electrodes [12].

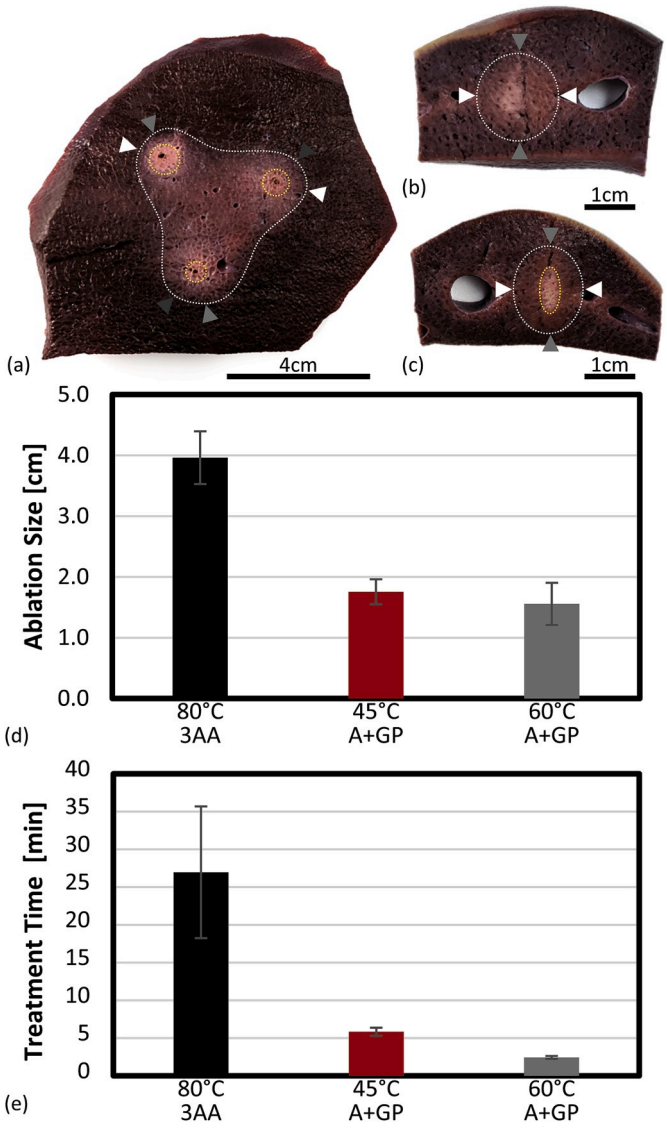


**Fig. 5.** ETT ablations created using the (a) 3AA and (b–c) A + GP configurations. The ETT ablation zones are outlined in white and thermal injury zones are outlined in yellow. Color matched arrow heads indicate locations where measurement were acquired for each configuration. (d) Ablation sizes and (e) treatment times were dependent on the applicator configuration and treatment protocol.

This study demonstrates the potential of ETT to mitigate these challenges. Notably, ETT treatments rapidly generated 4 cm ablation zones with energy delivery times of approximately 27 min without the need to relocate or retract the electrode applicators. Clinical treatment of 3 cm tumors with NK-IRE typically requires the placement of 4 applicators followed by multiple treat and retract cycles due to the 3000 V and 50 A constraints of the electronics. This limits electrode exposures to 1–2 cm, limits applicator spacing to 1–2 cm, requires multiple clinician interventions to reposition the applicators, and requires energy delivery times of approximately 35 min [13]. In this study, no additional intervention was needed once the 3 cm electrodes were placed.

The 75A current limit on the pulse generator used in this study was set as a precautionary safety measure as part of an automated arc detection and prevention scheme given its wide use in *in vitro, ex vivo*,

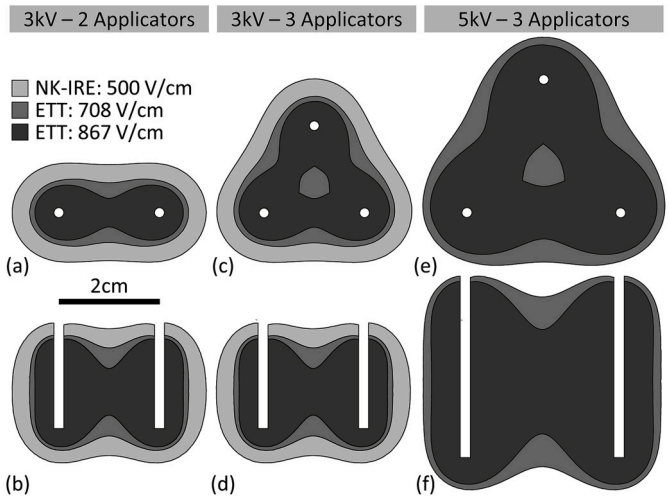


**Fig. 6.** Predicted treatment zones utilizing (a–b) two applicators with the NK-IRE maximum 1.5 cm electrode exposure and 2.0 cm center-to-center spacing with 3 kV waveforms. Larger treatment areas can be created via (c–d) three applicator approaches, but treatment depth is limited in NK-IRE by maximum output current limitations. (e–f) ETT enables the use of higher voltages (5 kV), electrode exposures (3 cm), and center-to-center spacing (3 cm) to create larger treatment zones without repositioning applicators. However, treatment parameters must be selected carefully to prevent under-treatment in the central region between the three applicators.

and *in vivo* studies within the laboratory. There were no technological limitations preventing the use of longer electrode exposures and higher treatment currents.

For 5000 V ETT treatments, thermal effects are a substantial concern. A challenge with pulsed electric field therapies is the feed forward process by which elevated tissue temperatures due to energy delivery increase tissue conductivity which increases the rate of tissue heating. When uncontrolled, a temperature increase of 76 °C was observed from a baseline of 20 °C (Fig. 3a) with treatments between the next sequential probe pair rapidly reaching 100 °C resulting in steam ejection from the applicator site. While this may not be a substantial concern to clinicians who typically utilize thermal ablation modalities, NK-IRE is generally discussed as a non-thermal ablation technique [7,10,11,39]. As temperatures are typically not recoded during these NK-IRE interventions, it is not possible to definitively determine the extent of thermal injury induced in prior studies, however, thermal injury zones were observed adjacent to the applicator insertion path in *ex vivo* perfused liver studies [25]. As voltages increase in pursuit of the ability to treat larger tumors (e.g. greater than 3 cm) the extent of this thermal injury is likely to increase unless active measures are enacted.

The algorithm utilized in this study readily achieved stabile temperature control at relatively low (45 °C, Supplemental Fig. 4), moderate (60 °C, Supplemental Fig. 4), and relatively high (80 °C, Fig. 4) temperature set points. However, there were some challenges. Temperature profiles did vary between energized applicators in the 3AA. This was potentially due to slight variations in the placement of the temperature sensor and required an observer to switch which temperature value was being utilized by the algorithm. This process should be automated in the future to mitigate the potential for unwanted temperature spikes. In the 60 °C A + GP configuration tissue temperatures did not saturate at 60 °C in all treatments (Supplemental Fig. 1a). This was likely due to variations in the treatment current and the use of a maximum energy delivery rate (200 μs/s) which was insufficient to rapidly heat the tissue to the target set point before treatment completion. However, previous 5 kV studies using an A + GP applicator configuration readily achieved peak temperatures over 70 °C with energy delivery rates of 200 μs/s and 300 μs/s [12] indicating that the algorithm effectively mitigated the extreme temperatures possible in this applicator configuration.

An advantage to this temperature control scheme is that it allows for clinical flexibility and enables clinicians to balance concern of thermal injury to proximal critical structures with time constraints associated with anesthesia and operating room logistics. In clinical practice, incorporating temperature sensors within the electrodes may marginally increase the diameter of the applicators. However, larger (e.g. 15AWG, 1.45 mm) applicators are common for RFA and microwave ablation procedures and a larger diameter applicator may improve the rigidity over NK-IRE applicators.

While not investigated in this study, it is feasible to use a temperature sensor placed directly adjacent to critical structures near, but not within the desired treatment zone (e.g. the hepatic portal tract) and utilize this additional sensor to control the energy delivery rate and mitigate off target thermal injury.

Calculation of lethal electric field strengths for treatment planning purposes can be challenging from data acquired from treatments which utilize multiple adjacent applicators (e.g. 3AA). The electric field strength decreases rapidly along the geometric line which connects the center of the electrodes (Supplemental Fig. 2d) so relatively small changes in the ablation size (Fig. 5d) result in large deviations in the predicted lethal electric field strength (Fig. 5e). The use of the A + GP configuration enables a more accurate prediction of the lethal threshold for these ETT treatments because it results in spherical ablation zones and an electric field distribution which decays more slowly at distances approximately equivalent to the ablation margin. The lethal electric fields found here were moderately higher than those found for 5 kV treatments without temperature control (540–703 V/cm) [12] and future *in vivo* studies will be necessary to understand how discrete temperature set points affect treatment outcomes.

Simulations utilizing this data predict that when voltage and dose are held constant, these ETT treatments will produce smaller ablation zones than NK-IRE (Fig. 6) which typically has a lethal threshold in proximity to 500 V/cm. However, ETT is amenable the use of greater voltages, enabling larger applicator spacing, and greater currents, enabling larger electrode exposures, than possible with clinical NK-IRE systems. This ultimately yields larger ablation zones than feasible with NK-IRE which is limited to approximately 2.5 cm on edge according to the manufacturer's marketing materials. The 5 kV treatments administered here resulted in treatment zones measuring approximately 4 cm on edge and numerical simulations of 6 kV and 10 kV treatments (Supplemental Fig. 5) predict treatment zones measuring approximately 5 and 7 cm, respectively. The lethal thresholds for ETT may be further reduced when treatments are administered at physiological temperature [23,40] or with greater IET doses (0.02–0.08) [24,28] enabling the production of even larger treatment zones.

There are some important limitations to this study. A room temperature *ex vivo* liver perfusion model was utilized. While this tissue model has been validated against *in vivo* data for NK-IRE treatments [25], it has not yet been validated for ETT treatments. The tissue was perfused with PBS which has a relatively high conductivity compared to blood which may have increased Joule heating effects. Similarly, the baseline tissue temperature *in vivo* will be approximately 17 °C greater than those investigated here. This may result in larger treatment currents and will limit the maximum acceptable temperature change, so further optimization of these algorithms may be necessary. The ablations created using the three applicator array had a distinct tri-lobed appearance which was not spherical or elliptical in nature and this geometry must be accounted for in treatment planning. However, future pulse generators with higher output voltages may alleviate this issue (Supplemental Fig. 5). The numerical model for calculating lethal electric field thresholds used a dynamic function to account for instantaneous changes in conductivity [41–43], but did not account for the action of individual pulses, temperature changes, or thermal injury (Supplemental Fig. 6 - Supplemental Fig. 7). The data presented here should not be used for clinical treatment planning until these models can be compare to *in vivo* data. Mechanical perfusion of *ex vivo* tissue makes microscopic histologic analysis

challenging as changes (e.g. coagulative necrosis) are generally observable only for in situ ablations. Therefore measurements of ablation zones were based on measurements of gross tissue sections. *In vivo* confirmation via ultrasound, MRI, and histology will be necessary to validate the data generated here. Similarly, *in vivo* survival studies will be required to assess whether ETT treatments more safely spare adjacent anatomical structures than NK-IRE, MWA, or RFA.

## 5. Conclusion

This study demonstrates the ability of ETT waveforms and temperature control algorithms to rapidly and reproducibly create 4 cm ablations utilizing a 3 applicator array. Energy delivery was completed approximately 8 min faster than NK-IRE treatments intended to treat 3 cm tumors. Additionally, the ETT protocols were completed without the need for intervention to relocate applicators mid-treatment. When present, thermal injury zones in these treatments were limited to regions directly adjacent to the electrodes despite the use of 5000 V waveforms. The single applicator and multi-applicator arrays demonstrated may enable to treatment of complex tumor geometries and the flexibility of ETT temperature control may provide a malleable intervention which gives clinicians robust control over the ablation modality, treatment time, and safety profile.

## Declaration of competing interest

MBS, CCF, RAP, and LX have issued or pending patents related to IRE and H-FIRE technologies. MBS recieves royalties from AngioDynamics Inc. The other authors have no conflicts of interest to declare.

## Acknowledgement

The authors would like to thank the UNC/NCSU Joint Department of Biomedical Engineering for their support of this work via provisioning of startup funding. Additional funding was supplied by the North Carolina State University Chancellor's Innovation Fund

## Appendix A. Supplementary data

Supplementary data to this article can be found online at https://doi.org/10.1016/j.compbiomed.2020.103807.

## References

[1] F.H. Cornelis, et al., A comparative study of ablation boundary sharpness after percutaneous radiofrequency, cryo-, microwave, and irreversible electroporation ablation in normal swine liver and kidneys, Cardiovasc. Intervent. Radiol. 40 (10) (Oct 2017) 1600–1608, https://doi.org/10.1007/s00270-017-1692-3.

[2] L.S. Poulou, E. Botsa, I. Thanou, P.D. Ziakas, L. Thanos, Percutaneous microwave ablation vs radiofrequency ablation in the treatment of hepatocellular carcinoma, World J. Hepatol. 7 (8) (2015) 1054.

[3] S.J. Lee, L.T. Choyke, J.K. Locklin, B.J. Wood, Use of hydrodissection to prevent nerve and muscular damage during radiofrequency ablation of kidney tumors, J. Vasc. Intervent. Radiol. 17 (12) (2006) 1967–1969.

[4] A.J. Moreland, et al., Evaluation of a thermoprotective gel for hydrodissection during percutaneous microwave ablation: in vivo results, Cardiovasc. Intervent. Radiol. 38 (3) (2015) 722–730.

[5] T.P. Kingham, et al., Ablation of perivascular hepatic malignant tumors with irreversible electroporation, J. Am. Coll. Surg. 215 (3) (2012) 379–387.

[6] H.J. Scheffer, et al., Irreversible electroporation for nonthermal tumor ablation in the clinical setting: a systematic review of safety and efficacy, J. Vasc. Intervent. Radiol. : J. Vasc. Intervent. Radiol. 25 (7) (Jul 2014) 997–1011, https://doi.org/10.1016/j.jvir.2014.01.028, quiz 1011.

[7] R.E. Neal, et al., In vivo characterization and numerical simulation of prostate properties for non-thermal irreversible electroporation ablation, Prostate 74 (5) (2014) 458–468.

[8] P.A. Garcia, J.H. Rossmeisl Jr., T.L. Ellis, R.V. Davalos, Nonthermal irreversible electroporation as a focal ablation treatment for brain cancer, in: Tumors of the Central Nervous System, vol. 12, Springer, 2014, pp. 171–182.

[9] A. Golberg, M.L. Yarmush, Nonthermal irreversible electroporation: fundamentals, applications, and challenges, IEEE Trans. Biomed. Eng. 60 (3) (Mar 2013) 707–714, https://doi.org/10.1109/TBME.2013.2238672.

[10] P.A. Garcia, et al., Non-thermal irreversible electroporation (N-TIRE) and adjuvant fractionated radiotherapeutic multimodal therapy for intracranial malignant glioma in a canine patient, Technol. Canc. Res. Treat. 10 (1) (Feb 2011) 73–83 [Online]. Available, http://www.ncbi.nlm.nih.gov/pubmed/21214290.

[11] E. Maor, A. Ivorra, B. Rubinsky, Non thermal irreversible electroporation: novel technology for vascular smooth muscle cells ablation, PloS One 4 (3) (2009) e4757.

[12] J.D. Kaufman, et al., High-frequency irreversible electroporation using 5,000-V waveforms to create reproducible 2- and 4-cm ablation zones - a laboratory investigation using mechanically perfused liver, J. Vasc. Intervent. Radiol. 31 (1) (2020) 162–168.e7, https://doi.org/10.1016/j.jvir.2019.05.009.

[13] R.C. Martin, 2nd, et al., Treatment of 200 locally advanced (stage III) pancreatic adenocarcinoma patients with irreversible electroporation: safety and efficacy, Ann. Surg. 262 (3) (Sep 2015) 486–494, https://doi.org/10.1097/SLA.0000000000001441, discussion 492-4.

[14] B. Mali, D. Miklavčič, G. Sersa, T. Jarm, Comparison of protocols for synchronized electroporation pulse delivery, in: 6th European Conference of the International Federation for Medical and Biological Engineering, Springer, 2015, pp. 586–589.

[15] A. Deodhar, et al., Irreversible electroporation near the heart: ventricular arrhythmias can be prevented with ECG synchronization, Am. J. Roentgenol. 196 (3) (2011) W330–W335.

[16] C.B. Arena, R.V. Davalos, Advances in therapeutic electroporation to mitigate muscle contractions, J. Membr. Sci. Technol. (2012), https://doi.org/10.4172/2155-9589.1000e102.

[17] M. Faroja, et al., Irreversible electroporation ablation: is all the damage nonthermal? Radiology 266 (2) (2013) 462–470.

[18] M.B. Sano, C.B. Arena, M.R. DeWitt, D. Saur, R.V. Davalos, In-vitro bipolar nano- and microsecond electro-pulse bursts for irreversible electroporation therapies, Bioelectrochemistry 100 (Dec 2014) 69–79, https://doi.org/10.1016/j.bioelechem.2014.07.010.

[19] C.B. Arena, M.B. Sano, M.N. Rylander, R.V. Davalos, Theoretical considerations of tissue electroporation with high-frequency bipolar pulses, IEEE Trans. Biomed. Eng. 58 (5) (May 2011) 1474–1482, https://doi.org/10.1109/TBME.2010.2102021.

[20] C.B. Arena, et al., High-frequency irreversible electroporation (H-FIRE) for non-thermal ablation without muscle contraction, Biomed. Eng. Online 10 (1) (2011) 102, https://doi.org/10.1186/1475-925X-10-102.

[21] M.B. Sano, M.R. DeWitt, S.D. Teeter, L. Xing, Optimization of a single insertion electrode array for the creation of clinically relevant ablations using high-frequency irreversible electroporation, Comput. Biol. Med. 95 (Apr 1 2018) 107–117, https://doi.org/10.1016/j.compbiomed.2018.02.009. English.

[22] M.B. Sano, R.E. Fan, G.L. Hwang, G.A. Sonn, L. Xing, Production of spherical ablations using nonthermal irreversible electroporation: a laboratory investigation using a single electrode and grounding pad, J. Vasc. Intervent. Radiol. : J. Vasc. Intervent. Radiol. 27 (9) (Sep 2016) 1432–1440, https://doi.org/10.1016/j.jvir.2016.05.032, e3.

[23] R.A. Petrella, C.C. Fesmire, J.A. Kaufman, N. Topasna, M.B. Sano, Algorithmically controlled electroporation: a technique for closed loop temperature regulated pulsed electric field cancer ablation, in: IEEE Transactions on Biomedical Engineering, Press, 2020.

[24] M.B. Sano, C.C. Fesmire, M.R. DeWitt, L. Xing, Burst and continuous high frequency irreversible electroporation protocols evaluated in a 3D tumor model, Phys. Med. Biol. 63 (13) (Jul 6 2018) 135022, https://doi.org/10.1088/1361-6560/aacb62.

[25] S. Bhonsle, et al., Characterization of irreversible electroporation ablation with a validated perfused organ model, J. Vasc. Intervent. Radiol. : J. Vasc. Intervent. Radiol. 27 (12) (Dec 2016) 1913–1922, https://doi.org/10.1016/j.jvir.2016.07.012, e2.

[26] T.J. O'Brien, et al., Effects of internal electrode cooling on irreversible electroporation using a perfused organ model, Int. J. Hyperther. 35 (1) (Jan 1 2018) 44–55, https://doi.org/10.1080/02656736.2018.1473893. English.

[27] M.B. Sano, R.E. Neal, , II, P.A. Garcia, D. Gerber, J. Robertson, R.V. Davalos, Towards the creation of decellularized organ constructs using irreversible electroporation and active mechanical perfusion, Biomed. Eng. Online 9 (DEC 10 2010 2010), https://doi.org/10.1186/1475-925X-9-83.

[28] J.D. Kaufman, M.R. DeWitt, E. Lattouche, C.C Fesmire, J. Swet, R. Kirks, E. Baker, D. Vrochides, D. Iannitti, I. McKillop, R.V. Davalos, M.B. Sano, Simplified Non-Thermal Tissue Ablation With A Single Insertion Device Enabled By Bipolar High-Frequency Pulses, IEEE Transactions on Biomedical Engineering (2019), https://doi.org/10.1109/TBME.2019.2954122. In press.

[29] S.N. Goldberg, M.C. Stein, G.S. Gazelle, R.G. Sheiman, J.B. Kruskal, M.E. Clouse, Percutaneous radiofrequency tissue ablation: optimization of pulsed-radiofrequency technique to increase coagulation necrosis, J. Vasc. Intervent. Radiol. 10 (7) (1999) 907–916.

[30] M.B. Sano, M.R. DeWitt, S. Teeter, L. Xing, Optimization of a single insertion electrode array for the creation of clinically relevant ablations using high-frequency irreversible electroporation, Comput. Biol. Med. 95 (2018) 107–117, https://doi.org/10.1016/j.compbiomed.2018.02.009.

[31] 1 D. Miklavcic, D. Semrov, H. Mekid, L.M. Mir, in: A Validated Model of in Vivo Electric Field Distribution in Tissues for Electrochemotherapy and for DNA Electrotransfer for Gene Therapy, vol. 1523, *English), Biochim. Biophys.* Acta-Gen. Subj., Sep 2000, pp. 73–83 [Online]. Available: <Go to ISI>://000089920500010.

[32] P. Garcia, et al., Intracranial nonthermal irreversible electroporation: in vivo analysis, J. Membr. Biol. 236 (Jul) (2010) 127–136.

[33] G.C. Van Rhoon, T. Samaras, P.S. Yarmolenko, M.W. Dewhirst, E. Neufeld, N. Kuster, CEM43° C thermal dose thresholds: a potential guide for magnetic resonance radiofrequency exposure levels? Eur. Radiol. 23 (8) (2013) 2215–2227.

[34] M.W. Dewhirst, B. Viglianti, M. Lora-Michiels, M. Hanson, P. Hoopes, Basic principles of thermal dosimetry and thermal thresholds for tissue damage from hyperthermia, Int. J. Hyperther. 19 (3) (2003) 267–294.
[35] P.S. Yarmolenko, et al., Thresholds for thermal damage to normal tissues: an update, Int. J. Hyperther. 27 (4) (2011) 320–343.
[36] G. Narayanan, S. Bhatia, A. Echenique, R. Suthar, K. Barbery, J. Yrizarry, Vessel patency post irreversible electroporation, Cardiovasc. Intervent. Radiol. 37 (6) (2014) 1523–1529.
[37] C. Niessen, et al., Percutaneous Irreversible Electroporation: long-term survival analysis of 71 patients with inoperable malignant hepatic tumors, Sci. Rep. 7 (2017) 43687.
[38] M. Lundy, M. Garland-Kledzik, P. Shen, Arterio-enteric fistula after irreversible electroporation, Am. Surg. 85 (1) (2019) E55–E57.
[39] A. Golberg, M.L. Yarmush, Nonthermal irreversible electroporation: fundamentals, applications, and challenges, IEEE Trans. Biomed. Eng. 60 (3) (2013) 707–714.
[40] C.C. Fesmire, R.A. Petrella, C.A. Fogle, D. Gerber, L. Xing, M.B. Sano, Temperature dependence of high frequency irreversible electroporation evaluated in a 3D tumor model, Ann. Biomed. Eng. (2020), https://doi.org/10.1007/s10439-019-02423. In press.
[41] P.A. Garcia, B. Kos, J.H. Rossmeisl Jr., D. Pavliha, D. Miklavcic, R.V. Davalos, Predictive therapeutic planning for irreversible electroporation treatment of spontaneous malignant glioma, Med. Phys. 44 (9) (Sep 2017) 4968–4980, https://doi.org/10.1002/mp.12401.
[42] R.E. Neal II, et al., Simulation of in vivo irreversible electroporation renal ablations, in: 6th European Conference of the International Federation for Medical and Biological Engineering, Springer, 2015, pp. 813–816.
[43] R.E. Neal, et al., In vivo irreversible electroporation kidney ablation: experimentally correlated numerical models, IEEE (Inst. Electr. Electron. Eng.) Trans. Biomed. Eng. 62 (2) (2014) 561–569.